HHS Public Access

Author manuscript

J Mol Biol. Author manuscript; available in PMC 2024 February 23.

Published in final edited form as:

J Mol Biol. 2024 February 15; 436(4): 168409. doi:10.1016/j.jmb.2023.168409.

Molecular Determinants of PQBP1 Binding to the HIV-1 Capsid Lattice

Juliana Piacentini[1], **Dale S. Allen**[3], **Barbie K. Ganser-Pornillos**[1,2], **Sumit K. Chanda**[3], **Sunnie M. Yoh**[3], **Owen Pornillos**[1,2]

[1]University of Virginia, Department of Molecular Physiology & Biological Physics, Charlottesville, VA, USA

[2]University of Utah, Department of Biochemistry, Salt Lake City, UT, USA

[3]The Scripps Research Institute, Department of Immunology and Microbiology, La Jolla, CA, USA

Abstract

Human immunodeficiency virus type 1 (HIV-1) stimulates innate immune responses upon infection, including cyclic GMP-AMP synthase (cGAS) signaling that results in type I interferon production. HIV-1-induced activation of cGAS requires the host cell factor polyglutamine binding protein 1 (PQBP1), an intrinsically disordered protein that bridges capsid recognition and cGAS recruitment. However, the molecular details of PQBP1 interactions with the HIV-1 capsid and their functional implications remain poorly understood. Here, we show that PQBP1 binds to HIV-1 capsids through charge complementing contacts between acidic residues in the N-terminal region of PQBP1 and an arginine ring in the central channel of the HIV-1 CA hexamer that makes up the viral capsid. These studies reveal the molecular details of PQBP1′s primary interaction with the HIV-1 capsid and suggest that additional elements are likely to contribute to stable capsid binding.

Keywords

virus capsid; innate immune response; host factors; charge complementation

Correspondence to Sunnie M. Yoh and Owen Pornillos: syoh@scripps.edu (S.M. Yoh), owen@biochem.utah.edu (O. Pornillos).

CRediT authorship contribution statement

Juliana Piacentini: Conceptualization, Investigation, Methodology, Validation, Visualization, Writing – original draft, Writing – review & editing. **Dale S. Allen:** Investigation, Methodology, Validation, Writing – review & editing. **Barbie K. Ganser-Pornillos:** Funding acquisition, Investigation, Methodology, Validation, Writing – review & editing. **Sumit K. Chanda:** Conceptualization, Funding acquisition, Supervision, Writing – review & editing. **Sunnie M. Yoh:** Conceptualization, Funding acquisition, Investigation, Methodology, Supervision, Validation, Writing – review & editing. **Owen Pornillos:** Conceptualization, Funding acquisition, Investigation, Methodology, Supervision, Validation, Visualization, Writing – original draft, Writing – review & editing.

DECLARATION OF COMPETING INTEREST

The authors declare that they have no known competing financial interests or personal relationships that could have appeared to influence the work reported in this paper.

Appendix A. Supplementary data

Supplementary data to this article can be found online at https://doi.org/10.1016/j.jmb.2023.168409.

Introduction

Cyclic GMP-AMP synthase (cGAS) is a pattern recognition receptor (PRR) that induces an interferon response upon recognition of cytosolic double-stranded DNA (dsDNA).[1–3] The cGAS pathway functions as a first-line defense against DNA and RNA viruses, including HIV-1.[4–7] Reverse-transcribed HIV-1 DNA is one of the pathogen-associated molecular patterns (PAMPs) that can be recognized by cGAS, but these nascent transcripts are normally sequestered and protected within the viral capsid. Activation of cGAS during HIV-1 infection requires polyglutamine binding protein 1 (PQBP1), which binds to the capsid and recruits cGAS to the reverse-transcribing viral particle.[8,9]

PQBP1 is an intrinsically disordered protein (IDP) of 265 amino-acid residues (Figure 1A) that is found both in the cell nucleus and cytoplasm.[10–12] Being an IDP, PQBP1 lacks a well-ordered globular fold, apart from a small WW domain (Figure 1B);[10,12,13] this property makes it challenging to define the protein's structure–function correlates. Previous studies have shown that PQBP1 recognizes the HIV-1 capsid through its N-terminal region, whereas cGAS recruitment and activation requires the WW domain as well as elements in the C-terminal region (Figure 1A).[8,9] However, many details of these separate activities and how they mechanistically integrate to enable HIV-dependent cGAS signaling remain unknown.

In this study, we focus on understanding the molecular mechanism by which PQBP1 binds and recognizes the HIV-1 capsid. Recent studies have revealed that PQBP1 binding to the capsid requires Arg18 in HIV-1 CA, the viral protein that makes up the capsid subunits.[9] Six Arg18 residues form a ring or annulus within the central channel of the CA hexamer, which is one of the oligomeric building blocks of the capsid. The Arg18 ring is a well-characterized binding site for acidic ligands, including nucleotide triphosphates,[14] the capsid-stabilizing factor inositol hexakisphosphate (IP_6),[15,16] and the transport factor FEZ1, which contains poly-glutamate motifs.[17] The N-terminal (Nt) region of PQBP1 also contains acidic motifs,[9] leading to the inference that, analogous to the above ligands, PQBP1 also binds the Arg18 ring via charge complementation. However, direct demonstration of this interaction has not been reported and the corresponding amino-acid residue determinants have not been thoroughly defined. Likewise, whether and how other regions of PQBP1 contribute to productive capsid recognition have not been elucidated. To address these gaps in knowledge, we used purified PQBP1 proteins and disulfide-stabilized HIV-1 CA assemblies to reconstitute PQBP1-capsid complexes in vitro for biochemical and structural analyses. Our results uncover the molecular details of the minimal binding interaction between PQBP1 Nt and the HIV-1 CA hexamer. Furthermore, we also report evidence that PQBP1 regions outside of Nt contribute to stable capsid binding. We propose that, similar to other well-characterized factors that target the HIV-1 capsid, PQBP1 likely requires avidity for functional capsid recognition.

Results

PQBP1 Nt directly binds the HIV-1 CA hexamer

We purified recombinant, full-length PQBP1 (Supplementary Figure S1A) and characterized its binding to soluble, disulfide-crosslinked HIV-1 CA hexamers. As described before,

the crosslinked CA hexamer is held together by designed disulfides (A14C/E45C), which, in combination with mutations (W184A/M185A) that destabilize the extended capsid lattice, allow preparation of discrete hexamers in solution.[18] These hexamers have been used in many studies of HIV-1 capsid-binding factors. To measure binding, we utilized nanodifferential scanning fluorimetry (nanoDSF), a technique used to measure the thermostability of folded proteins. In this experiment, protein unfolding is indicated by the shift in peak Trp fluorescence as these residues transition from hydrophobic (protein interior) to hydrophilic (exposed to solvent) environments. Since the disulfide-stabilized CA hexamers contain Trp residues only in the N-terminal domain (NTD), their nanoDSF profiles report on the unfolding of the central NTD ring that contains the Arg18 ring. The hexamer displayed a single unfolding transition, with an apparent melting temperature (T_m) of 50.7 ± 0.5 °C (Supplementary Figure S1B, dark blue curves). On the other hand, purified PQBP1, which contains three Trp residues, displayed a non-canonical nanoDSF profile indicative of a largely unfolded state in solution (Supplementary Figure S1B, orange curves). A sample containing both proteins revealed a shift in CA's apparent T_m by around 2 °C (Supplementary Figure S1B, blue curves). This degree of thermostabilization in nanoDSF and DSF assays is generally accepted to indicate a direct binding interaction.[19]

To begin mapping the binding determinants in PQBP1, we tested various fragments for their ability to increase thermostability of the CA hexamer. Because PQBP1 is an IDP, we used functional annotations (e.g., Figure 1A) rather than structurally-defined domains for fragment design (Figure 2A). Results show that the PQBP1 fragment spanning Nt (residues 1–46) shifted the apparent T_m of the hexamer (Figure 2B, compare magenta and black curves). In contrast, the WW domain, polar-rich domain (PRD) and C-terminal (Ct) fragments had no effect (Figure 2B, compare green, blue, and orange curves to black). Dose-response curve fitting showed that Nt binds the hexamer with an apparent dissociation constant (K_d) of around 500 nM (Figure 2C and Table 1), indicating a relatively high-affinity complex in vitro. As noted previously,[9] Nt contains clusters of acidic residues, and in particular two tripeptide motifs ($_{25}$EEE$_{27}$ and $_{34}$DDD$_{36}$). To determine if these motifs contribute to the interaction, we tested an Nt construct harboring GGG substitutions for each of the motifs (Figure 3A,C). The mutant Nt did not bind the CA hexamer.

The Arg18 ring of the HIV-1 CA hexamer has also been implicated in PQBP1 binding,[9] so we performed the same experiments with an R18A mutant of the hexamer (Figure 3B,C). None of the PQBP1 fragments, including Nt, induced thermostabilization in this case, confirming the importance of Arg18 in PQBP1 binding to the CA hexamer.

Finally, we used cryoEM to compare 2D class averages of the non-mutated CA (Arg18) and R18A mutant hexamers. We observed extra density within the central channel of the non-mutated hexamer but not the R18A hexamer (red arrows in Figure 3D). These results are consistent with the interpretation that, similar to other acidic ligands,[14–17] PQBP1 Nt binds to the ring of six Arg18 residues located within the hexamer channel.

CryoEM structure of the HIV-1 CA hexamer bound to PQBP1 Nt

To directly visualize binding of PQBP1 Nt to the HIV-1 CA hexamer, we vitrified samples in cryoEM grids, collected cryoimages, and solved the structure by using the single-particle

averaging technique (Supplementary Figure S2A and Table 2). The hexamers had a marked preferred orientation on the grids, and so we combined particle sets picked from images collected at 0° and 30° tilts. An initial consensus map of the CA hexamer bound to Nt was refined to a nominal resolution of 3.3 Å (according to the gold-standard 0.143 cut-off) without imposing symmetry (C1) (Supplementary Figure S2B and Table 2). The CA residues are very well-defined, indicating that the map is of high quality (Supplementary Figure S2C). The extra density within the central channel that we attribute to Nt appears as an elongated blob that has proteinaceous features but is less well-defined than CA densities (Figure 4A,B). The peptide density is not 6-fold symmetric. Our interpretation is that even though the ordered peptide segment is only 3% that of the CA subunits, it is sufficiently well-ordered to contribute to the alignment. However, the peptide remains the average of multiple bound orientations, indicating that the 6-fold symmetric features of the CA ring still dominates particle alignment.

In an attempt to improve the Nt densities, we tested a variety of post-alignment processing and 3D classification strategies. None had sufficient power to resolve a unique peptide orientation, but 3D variability analysis (3DVA)[20] (see Methods and Supplementary Figure S3 for details) highlighted some key features. Firstly, the consensus map indicates a single peptide chain bound within the central channel of the hexamer. We could observe evenly spaced ridges in the peptide density (dashed lines in Figure 4B), which we interpret to be consistent with a helical configuration. Although requiring further confirmation, this feature would be consistent with the typical IDP behavior of binding-induced folding into canonical secondary structural motifs when complexed with their partners.[21] In principle, the density can also accommodate two chains in elongated or strand configuration. However, 2D class averages (face views only) confirmed that the hexamers predominantly contain a single density feature in the central channel, and only a very small proportion (<1%) contains two peptide densities (Supplementary Figure S3D). Secondly, although the peptide density in the consensus map is centered within the hexamer, the peptide is actually positioned asymmetrically. This key point is illustrated by modes of variation, derived from 3DVA, that run along vectors perpendicular to the central axis of the hexamer channel (Figure 4C). Maps reconstructed from the extreme positions of these vectors (Supplementary Figure S3A–C and Table 2) show that the long axis of the peptide does not coincide with the channel center (Figure 4D). Thirdly, the maps clearly indicate direct contacts to the CA Arg18 sidechains. Notably, the 3DVA subset maps show contacts to only one or two, and not all six, Arg18 residues (Figure 4D, red asterisks).

In summary, our cryoEM structure empirically establishes that Nt indeed binds within the CA hexamer channel and directly contacts Arg18. Unfortunately, resolving the bound peptide structure within its 6-fold symmetric binding site is pushing the limits of the single-particle averaging technique, and will have to await further studies.

A tri-aspartate motif mediates PQBP1 Nt binding to the HIV-1 CA hexamer

Assuming an a-helix configuration, the bound Nt density would be consistent with at most 15 amino-acid residues, i.e., one-third of Nt. To more precisely determine the portion of Nt that binds the hexamer, we used nanoDSF to test 15-mer peptides with 10-residue

overlaps (Figure 5A). Results indicate that 15-mer peptides containing either the EEE or DDD motifs displayed measurable binding (Figure 5A and Supplementary Figure S4B), but two fragments containing the DDD motif bound with the highest affinities (85 nM for 15–5 and 54 nM for 15–6) (Figure 5B and Table 1). Experiments with overlapping 10-mer and 20-mer fragments produced similar results (Supplementary Figure S4A,B). To confirm the importance of Asp over Glu, we generated variants of peptide 15–6 (EIIAE DYDDD PVDYE), which bound the hexamer with highest affinity. As expected from results with Nt, substitution of the DDD motif for AAA abolished binding (Supplementary Figure S4C). Interestingly, a peptide containing only Asp residues (DIIAD DYDDD PVDYD) afforded higher thermostabilization of the CA hexamer compared to a peptide containing only Glu residues (EIIAE EYEEE PVEYE) (Supplementary Figure S4C). These results suggest that, in addition to the charge complementing interactions with Arg18, steric requirements help to define binding specificity of peptide ligands to the CA hexamer, at least in vitro.

To confirm the importance of the above acidic motifs in Nt for PQBP1-mediated sensing of HIV-1, we assayed for HIV-dependent ISG54 induction in the monocyte-like THP-1 cell line differentiated with PMA (phorbol 12-myristate-13-acetate), an established model system for human macrophages (Figure 5C). Cells stably expressing the indicated siRNA-resistant PQBP1-eYFP constructs were transfected with siRNA against endogenous PQBP1, then infected with HIV-1, followed by RT-qPCR analysis for ISG54 expression (see Methods for details). As previously shown,[9] control experiments with cells expressing wild type, full-length (FL) PQBP1-eYFP induced > 4-fold higher ISG54 mRNA expression compared to mock-infected cells (positive control), whereas the Nt-deletion mutant (ΔNt) had attenuated (<2-fold) response (negative control). We then tested E-to-G and D-to-G full-length PQBP1-eYFP mutant constructs, in which either the $_{25}$EEE$_{27}$ or $_{34}$DDD$_{36}$ motif was substituted for GGG. Both mutants induced ISG54 levels comparable to ΔNt. Western blotting confirmed that all PQBP1-eYFP constructs expressed at comparable levels (Figure 5D). These data confirm the importance of the acidic motifs in Nt for PQBP1-mediated innate immune responses to HIV-1. Taken together, our aggregate data also indicate that the pronounced difference between DDD and EEE in context of hexamer binding in vitro is attenuated in the cellular context. Our interpretation is that functional binding in cells requires both acidic motifs (see also Discussion).

Binding of PQBP1 to the HIV-1 capsid lattice

In cells, the functional target of PQBP1 is the assembled capsid, and indeed PQBP1 is shown to colocalize with incoming HIV-1 cores.[9] We therefore extended our binding studies by using full-length recombinant PQBP1 protein and HIV-1 capsid-like assemblies in vitro. Although IP_6-induced HIV-1 CA fullerene cones are more accurate mimics of actual viral capsids[22], our results with the hexamer indicated that PQBP1 binding will be inhibited by the mM levels of IP_6 that is present in these in vitro assemblies. Experiments were thus performed with A14C/E45C HIV-1 CA tubes (lacking the W814A/M185A mutations of the soluble, crosslinked CA hexamer) because these tubes can be reconstituted in almost any buffer solution (i.e., without IP_6) once the disulfide crosslinks form.[23] The disulfide-crosslinked tubes are established to be functional mimics of the HIV-1 capsid and have been used in many published pull-down binding studies. We incubated CA tubes with

full-length recombinant PQBP1 (with PQBP1 at 6-fold excess over CA hexamers), and then assessed binding by visualizing the protein fraction associated with pelleted CA tubes after centrifugation. As shown in Figure 6A (top row), substantially greater amounts of PQBP1 pelleted with CA tubes than without. Densitometry quantification indicated that 17 ± 6% (N = 9) of input PQBP1 pelleted with the CA tubes (Figure 6B), which is the theoretical saturation point assuming 1 binding site per CA hexamer. However, this number does not take into account contributions from non-specific binding. To estimate non-specific binding, we used the Nt-deletion and DE-to-G PQBP1 mutants, which pelleted with CA tubes at lower levels than wild-type PQBP1 (Figure 6A, middle two rows; quantified in Figure 6B). Assuming that wild-type PQBP1 has similar levels of non-specific binding to the CA tubes as the mutants, our combined pull-down results indicate that the PQBP1 molecules occupy around half of the available sites in the CA tubes, which in our view is reasonably efficient binding in vitro.

Interestingly, the Nt peptide did not bind CA tubes efficiently in this experiment, with only ~1% of input found in the pellet (Figure 6A, bottom row; quantified in Figure 6B). This result was unexpected, given Nt's apparent nM-level affinity for soluble CA hexamers in the nanoDSF experiments (Figure 2C). We surmised that Nt may dissociate from the CA tubes during centrifugation or that the central channel of the CA hexamer may be more resistant to peptide insertion in context of the assembled capsid lattice. We also performed a competition experiment in which equal amounts of Nt and full-length PQBP1 protein were incubated with the CA tubes prior to centrifugation. Results show diminution of pellet-associated full-length PQBP1 to background levels, which is consistent with binding competition (Figure 6C). Altogether, these data suggest that other regions of PQBP1, outside of Nt, are likely contributing to stable association of the full-length protein with the CA tubes. This result is reminiscent of TRIM5α: the principal binding interaction between CA and the TRIM5α capsid-binding module (the SPRY domain) is insufficient for stable binding to the assembled capsid lattice and requires contributions from other regions of the protein (reviewed by[24]).

Discussion

Our finding that Nt binds to the central channel of the CA hexamer provides a formal biochemical proof that PQBP1 is an HIV-1 capsid-binding protein, because the hexamer only exists in context of an assembled capsid. Our results also indicate that binding involves charge complementation between acidic residues in PQBP1 and the basic Arg18 ring in the central channel of the HIV-1 CA hexamer. Other host cell factors, including nucleotide triphosphates, IP_6, and FEZ1,[14–17] have been previously shown to bind to the Arg18 site via charge interactions. The addition of PQBP1 to the list highlights the importance of the Arg18 ring in HIV-1 capsid multifunctionality.

While our biochemical and structural data show that a tri-aspartate (DDD) motif in context of a small peptide represents the "minimal" PQBP1 binding element for the HIV-1 CA hexamer, the surrounding sequences are also clearly important. Specifically, a 46-mer peptide (Nt) binds with 10-fold weaker affinity to the CA hexamer than a 15-mer peptide. We surmise that this difference might be explained by the need to thread the peptide through the hexamer channel. Since the DDD motif is located in the middle of both Nt and the 15–6

peptide, binding would be more inefficient with the former because more residues will need to be threaded, increasing the probability of dissociation before the DDD motif can make contact with the Arg18 ring. This model can explain why multiple acidic motifs are found in both PQBP1 and FEZ1, i.e., to maintain productive contacts. Furthermore, our cryoEM structure suggests that the bound portion of Nt might fold into a helix. Although pending confirmation, binding-induced folding of PQBP1 would contribute additional stabilization to the interaction. We envision that PQBP1 acts in analogy to a grapnel or grappling hook, and that the Nt peptide segment that we observe in our cryoEM map represents a secure anchor point for PQBP1. Our observation of a minor subpopulation of hexamers containing two peptide densities can be interpreted as a hairpin configuration of Nt in an intermediate stage of insertion into the hexamer channel.

In cells, small molecule ligands for the Arg18 ring are thought to be at considerable excess over protein factors (e.g., IP_6 is estimated at 20 μM or more, and nucleotide triphosphates are collectively at around 10 mM).[25–27] These numbers indicate that productive protein binding to the HIV-1 capsid is not just determined by simple thermodynamic parameters. Indeed, many protein factors are now shown to stably bind to the HIV-1 capsid through avidity, and an important emerging concept is that the capsid acts as a multivalent recruitment platform for both pro-viral and anti-viral proteins.[24,28–36] Along these lines, we find that the PQBP1 Nt peptide does not sustainably bind to HIV-1 CA tubes to withstand centrifugation, whereas full-length PQBP1 does. We propose, in line with other capsid-binding factors, that other regions of PQBP1 outside of Nt also promote stable binding through avidity. Further studies are now required to delineate these regions in PQBP1 and determine how they promote capsid recognition and eventual cGAS activation.

Methods

Protein production

Full-length PQBP1 protein was sub-cloned into pET16b (Novagen) with a C-terminal His-tag and Gly-Gly linker. Transformed BL21(DE3) E. coli cells were induced mid-log phase with 1 mM IPTG for 4.5 h. Cells were pelleted, resuspended in buffer (50 mM Tris, pH 8.0, 500 mM NaCl, 1 mM TCEP) supplemented with a protease inhibitor tablet (Roche), and then lysed by a combination of lysozyme treatment and sonication. The soluble fraction was filtered into a gravity column packed with Ni-NTA beads (Qiagen) and incubated for 30 min at 4 °C. Following a wash of the beads, protein was eluted with resuspension buffer containing increasing concentrations of imidazole (50–300 mM). Appropriate fractions as determined by SDS-PAGE were pooled and dialyzed overnight at 4 °C into 20 mM Tris, pH 8.0, 100 mM NaCl, 1 mM TCEP. The sample was then loaded onto a HiTrap Q FF column (GE Healthcare) and eluted with a linear NaCl gradient. Protein fractions identified via SDS-PAGE were pooled for overnight dialysis at 4 °C into the final protein buffer of 20 mM Tris, pH 8.0, 100 mM NaCl, and either 1 mM TCEP or 5 mM β-mercaptoethanol. Samples were concentrated to 2–7 mg/mL and flash-frozen in liquid nitrogen for storage at −80 °C. The Nt-deletion (ΔNt) and DE-to-G PQBP1 mutant proteins were prepared in the same way. We found that the DE-to-G mutant was somehow prone to proteolysis, and thus the preparation contained significant amounts of lower-MW fragments. We judged this

mutant to be suitable for use in pull-down experiments because the CA band was still distinguishable in Coomassie-stained SDS-PAGE gels (Figure 6A).

Peptides corresponding to PQBP1 fragments (Supplementary Figure S4A) were obtained from a commercial source (Celltein) at > 95% purity (HPLC purification) and verified by mass spectrometry. All peptides were N-terminally acetylated and C-terminally amidated, except for Nt and those starting with proline, which were modified only at the C-terminus. Freeze-dried peptides were reconstituted in water or PQBP1 buffer to generate 30–50 mM stock solutions prior to use.

Disulfide-crosslinked A14C/E45C/W184A/M185A CA hexamers with or without the R18A mutation, and disulfide-crosslinked A14C/E45C CA tubes were prepared as previously described.[18].

Nanodifferential scanning fluorimetry

CA hexamers were briefly incubated (5 min) with PQBP1 constructs, loaded onto capillaries, and melting profiles (both raw curves and first derivative curves) were obtained using a Tycho NT.6 (NanoTemper), except for data shown in Figure 2B, which were obtained with a Prometheus (NanoTemper). Dose-response curves were obtained by serially diluting Nt peptide into 0.83 μM of hexamer (equivalent to 5 μM of CA subunits), or 15-mer peptide into 0.083 μM of hexamer. Each first derivative profile was fit as a sum of two Gaussian curves (corresponding to bound and unbound species) using Excel (Microsoft), as described[37]. Bound fractions were calculated from the area under each Gaussian curve. The dose–response data were then fit to a simple cooperative model, using the equation $y = y_{max} * [Nt]^n/(K_d^n + [Nt]^n)$, where K_d is the apparent dissociation constant, n is the apparent Hill coefficient, and y_{max} is the specific activity of CA.

Pull-down assays

CA tubes (50 μM in terms of CA subunits, which is equivalent to 8.3 μM in terms of CA hexamers) were incubated without or with 50 μM of indicated PQBP1 constructs for 1 h at room temperature. Pellet and supernatant fractions were separated in a microcentrifuge at maximum speed (~21,000 g) for 30 min at room temperature. Fractions were analyzed by using SDS-PAGE with Coomassie staining; pre-cast Mini-Protean 15-well 4–20% gradient gels (Biorad) and a standard protocol were used for uniform staining. Band quantification was performed with Fiji.[38].

ISG54 induction assay

THP-1 cells stably expressing both wild-type and mutant PQBP1-eYFP fusion proteins (with silent mutations conferring resistance to siRNAs targeted against endogenous PQBP1) were generated as described previously.[8] siRNA were introduced into PMA-differentiated THP-1 cells using Stemfect RNA transfection kits. Typically, 5 pmol of siRNAs and 0.17 μL of Stemfect were used per 2.5×10^4 cells. Forty-eight hours after siRNA transfection, cells were infected with VSV-G pseudotyped HIV-1 virus in the presence of VLP-VPX for 16 h, followed by RT-qPCR analysis for ISG54 expression.[4,8] The following siRNAs were used: siPQBP1 (5′-AAGCTCAGAAGCAGTAATGCA-3′), and non-targeting control (5′-AATC

GATCATAGGACGAACGC-3′). qPCR primers were described previously.[8] 5 ng of p24 or 2.5 RT units of HIV-1 were used per 25,000 cells in 100 μL of media.

CryoEM structure determination

CA hexamers (50 μM) were incubated with 3-fold excess of Nt peptide at room temperature for 1 h. Samples (4 μL) were diluted, and then applied to glow-discharged 1.2/1.3c-flat 300-mesh copper grids. The grids were briefly blotted manually, and then plunge-frozen in liquid ethane using a home-built device. CryoEM data were collected at the University of Virginia Molecular Electron Microscopy Core, using a Krios (ThermoFisher) operating at 300 kV and equipped with an energy filter and K3 direct detector (Gatan). Images were collected using EPU (ThermoFisher) at a pixel size of 1.08 Å in counting mode, with a total dose of 50 electrons/$Å^2$ over 40 frames, and target defocus of −0.5 to −2.5 μm. Two data sets were collected, one at 0° tilt (3,612 images) and a second at 30° tilt (936 images).

All image processing and map calculations were performed in cryoSPARC v.3.3.1–3.[39] Raw movies were corrected for beam-induced motion using MotionCor2.[40] CTF estimation was performed with CTFFIND4[41] for the 0° tilt data and Patch CTF for the 30° tilt data, both as implemented in cryoS-PARC. Initially, the two data sets were processed independently (Supplementary Figure S2A). After template-based picking, particles for ab initio calculation were selected through two or three rounds of reference-free 2D classification. Ab initio maps ($n = 4$) were calculated using default parameters and C6 symmetry applied. One class from each data set was selected then refined in a single round, with C1 symmetry. At this point, the two particle sets (659,056 total) were combined by reconstructing a single map with C1 symmetry. After local refinement, the particle set was separated into bound and unbound hexamers, using a 3D Variability Analysis (3DVA) run in cryoSPARC (as described below). The Nt-bound hexamer (312,788 particles) was first reconstructed without further alignment, and then subjected to one round of local refinement in C1 symmetry, yielding a final consensus map at nominal resolution of 3.3 Å (0.143 cutoff) (Supplementary Figure S2B).

The consensus map was further processed through another round of 3DVA, which defined alternative positions of the Nt peptide. Each new particle set was reconstructed without further alignment, resulting in two ligand-bound maps (154,820 and 157,280 particles), each at nominal resolution of 3.5 Å (at the 0.143 cut-off) (Supplementary Figure S3B,C). Note that odd and even particle assignments that were set after ab initio calculations were kept throughout this analysis, thus maintaining gold-standard conditions. We also confirmed that similar proportions of particles from tilted and untilted images were maintained. In principle, 3DVA could have been performed with each new map to define additional subsets, but ever-decreasing particle numbers became limiting.

3D variability analysis

Variability modes were calculated inside a mask that included the central part of the hexamer and excluded all CA density except for the β-hairpin and helix 1, with filter resolution set to 4 Å. Non-overlapping particle subsets were subsequently defined using a 3D Variability Display run in “intermediates” output mode, with number of frames set at 2 and width at 0.

Coordinate modeling

The consensus map was refined for one additional round with C6 symmetry applied. PDB 3H47,[18] which consists of a single chain of CA, was docked into this map, then refined in real space using Phenix,[42] with a single round of morphing and 3H47 as reference. The other five CA subunits were then fit by copying the first chain, and then docked into the C1 consensus map. After manual inspection and minor rebuilding in Coot,[43] real-space refinement was performed with non-crystallographic symmetry restraints. The Nt density was left unmodeled.

Data deposition

The consensus map has been deposited at the EMDB (EMD-41711) and the coordinate model of the CA hexamer has been deposited at the PDB (8TY6).

Supplementary Material

Refer to Web version on PubMed Central for supplementary material.

Acknowledgements

The University of Virginia Molecular Electron Microscopy Core facility was built in part with NIH grant G20-RR31199, U54-AI170856, R01-AI127302, R01-AI177265, R21-MH129205, T32-GM080186. Purchase of the Krios was funded in part by S10-RR025067. We especially thank K. Dryden and M. Purdy for assistance in cryoEM data collection, and M. Purdy for help with optimizing server and software set up. This study was funded by NIH U54-AI170856 (O.P. and B.K. G.-P.), and by NIH R01-AI127302, R01-AI177265, R21-MH129205, a CFAR Development Grant, and CHRP Basic Bio Pilot Grant BB19-SBMR-0 (S.M.Y and S.K.C.). J.P. was supported by NIH T32-GM080186.

References

1. Mosallanejad K, Kagan JC, (2022). Control of innate immunity by the cGAS-STING pathway. Immunol. Cell Biol 100, 409–423. [PubMed: 35485309]
2. Sun L, Wu J, Du F, Chen X, Chen ZJ, (2013). Cyclic GMP-AMP synthase is a cytosolic DNA sensor that activates the Type-I interferon pathway. Science 339, 786–791. [PubMed: 23258413]
3. Wu J, Sun J, Chen X, Du F, Shi H, Chen C, Chen ZJ, (2013). Cyclic-GMP-AMP is an endogenous second messenger in innate immune signaling by cytosolic DNA. Science 339, 826–830. [PubMed: 23258412]
4. Manel N, Hogstad B, Wang Y, Levy DE, Unutmaz D, Littman DR, (2010). A cryptic sensor for HIV-1 activates antiviral innate immunity in dendritic cells. Nature 467, 214–217. [PubMed: 20829794]
5. Gao D, Wu J, Wu Y, Du F, Aroh C, Yan N, Sun L, Chen ZJ, (2013). Cyclic GMP-AMP synthase is an innate immune sensor of HIV and other retroviruses. Science 341, 903–906. [PubMed: 23929945]
6. Lahaye X, Satoh T, Gentili M, Cerboni S, Conrad C, Hurbain I, El Marjou A, Lacabaratz C, Lelièvre J, Manel N, (2013). The capsids of HIV-1 and HIV-2 determine immune detection of the viral cDNA by the innate sensor cGAS in dendritic cells. Immunity 39, 1132–1142. [PubMed: 24269171]
7. Altfeld M, Gale M Jr., (2015). Innate immunity against HIV-1 infection. Nature Immunol 16, 554–562. [PubMed: 25988887]
8. Yoh SM, Schneider M, Seifried J, Soonthornvacharin S, Akleh RE, Olivieri KC, De Jesus PD, Ruan C, de Castro E, Ruiz PA, Germanaud D, des Portes V, García-Sastre A, König R, Chanda SK, (2015). PQBP1 is a proximal sensor of the cGAS-dependent innate response to HIV-1. Cell 161, 1293–1305. [PubMed: 26046437]

9. Yoh SM, Mamede JI, Lau D, Ahn N, Sánchez-Aparicio MT, Temple J, Tuckwell A, Fuchs NV, Cianci GC, Riva L, Curry H, Yin X, Gambut S, Simons LM, Hultquist JF, König R, Xiong Y, García-Sastre A, Böcking T, Hope TJ, Chanda SK, (2022). Recognition of HIV-1 capsid by PQBP1 licenses an innate immune sensing of nascent HIV-1 DNA. Mol. Cell 82, 2871–2884.e6. [PubMed: 35809572]
10. Rees M, Gorba C, de Chiara C, Bui TTT, Garcia-Maya M, Drake AF, Okazawa H, Pastore A, Svergun D, Chen YW, (2012). Solution model of the intrinsically disordered polyglutamine tract-binding protein-1. Biophys. J 102, 1608–1616. [PubMed: 22500761]
11. Mizuguchi M, Okazawa H, (2013). Structural study of polyglutamine tract-binding protein 1. Yakugaku Zasshi 133, 519–526. [PubMed: 23649393]
12. Tanaka H, Okazawa H, (2022). PQBP1: The key to intellectual disability, neurodegenerative diseases, and innate immunity. Int. J. Mol. Sci 23, 6227. [PubMed: 35682906]
13. Sudol M, McDonald CB, Farooq A, (2012). Molecular insights into the WW domain of the Golabi-Ito-Hall Syndrome protein PQBP1. FEBS Letter 586, 2795–2799.
14. Jacques DA, McEwan WA, Hilditch L, Price AJ, Towers GJ, James LC, (2016). HIV-1 uses dynamic capsid pores to import nucleotides and fuel encapsidated DNA synthesis. Nature 536, 349–353. [PubMed: 27509857]
15. Dick RA, Zadrozny KK, Xu C, Schur FKM, Lyddon TD, Ricana CL, Wagner JM, Perilla JR, Ganser-Pornillos BK, Johnson MC, Pornillos O, Vogt VM, (2018). Inositol phosphates are assembly co-factors for HIV-1. Nature 560, 509–512. [PubMed: 30069050]
16. Mallery DL, Márquez CL, McEwan WA, Dickson CF, Jacques DA, Anandapadamanaban M, Bichel K, Towers GJ, Saiardi A, Böcking T, James LC, (2018). IP6 is an HIV pocket factor that prevents capsid collapse and promotes DNA synthesis. eLife 7, e35335. [PubMed: 29848441]
17. Huang P, Summer BJ, Xu C, Perilla JR, Malikov V, Naghavi MH, Xiong Y, (2019). FEZ1 is recruited to a conserved cofactor site on capsid to promote HIV-1 trafficking. Cell Rep 28, 2373–2385.e7. [PubMed: 31422020]
18. Pornillos O, Ganser-Pornillos BK, Kelly BN, Hua Y, Whitby FG, Stout D, Sundquist WI, Hill CP, Yeager M, (2009). X-ray structures of the hexameric building block of the HIV capsid. Cell 137, 1282–1292. [PubMed: 19523676]
19. Gao K, Oerlemans R, Groves MR, (2020). Theory and applications of differential scanning fluorimetry in early-stage drug discovery. Biophys. Rev 12, 85–104. [PubMed: 32006251]
20. Punjani A, Fleet DJ, (2021). 3D variability analysis: resolving continuous flexibility and discrete heterogeneity from single particle cryo-EM. J. Struct. Biol 231, 107702
21. Malagrinò F, Diop A, Pagano L, Nardella C, Toto A, Gianni S, (2022). Unveiling induced folding of intrinsically disordered proteins – protein engineering, frustration and emerging themes. Curr. Opin. Struct. Biol 72, 153–160. [PubMed: 34902817]
22. Schirra RT, dos Santos NFB, Zadrozny KK, Kucharska I, Ganser-Pornillos BK, Pornillos O, (2023). A molecular switch modulates assembly and host factor binding of the HIV-1 capsid. Nature Struct. Mol. Biol 30, 383–390. [PubMed: 36759579]
23. Pornillos O, Ganser-Pornillos BK, Banumathi S, Hua Y, Yeager M, (2010). Disulfide bond stabilization of the hexameric capsomer of human immunodeficiency virus. J. Mol. Biol 401, 985–995. [PubMed: 20600115]
24. Ganser-Pornillos BK, Pornillos O, (2019). Restriction of HIV-1 and other retroviruses by TRIM5. Nature Rev. Microbiol 17, 546–556. [PubMed: 31312031]
25. Letcher AJ, Schell MJ, Irvine RF, (2008). Do mammals make all their own inositol hexakisphosphate? Biochem. J 416, 263–270. [PubMed: 18684107]
26. Diamond TL, Roshal M, Jamburuthugoda VK, Reynolds HM, Merriam AR, Lee KY, Balakrishnan M, Bambara RA, Planelles V, Dewhurst S, Kim B, (2004). Macrophage tropism of HIV-1 depends on efficient cellular dNTP utilization by reverse transcriptase. J. Biol. Chem 279, 51545–51553. [PubMed: 15452123]
27. Kennedy EM, Gavegnano C, Nguyen L, Slater R, Lucas A, Fromentin E, Schinazi RF, Kim B, (2010). Ribonucleoside triphosphates as substrate of human immunodeficiency virus type 1 reverse transcriptase in human macrophages. J. Biol. Chem 285, 39380–39391. [PubMed: 20924117]

28. Yap MW, Mortuza GB, Taylor IA, Stoye JP, (2007). The design of artificial retroviral restriction factors. Virology 365, 302–314. [PubMed: 17493656]

29. Javanbakht H, Diaz-Griffero F, Yuan W, Yeung DF, Li X, Song B, Sodroski J, (2007). The ability of multimerized cyclophilin A to restrict retrovirus infection. Virology 367, 19–29. [PubMed: 17574642]

30. Fribourgh JL, Nguyen HC, Matreyek KA, Alvarez FJD, Summers BJ, Dewdney TG, Aiken C, Zhang P, Engelman A, Xiong Y, (2014). Structural insight into HIV-1 restriction by MxB. Cell Host Microbe 16, 627–638. [PubMed: 25312384]

31. Goldstone DC, Walker PA, Calder LJ, Coombs PJ, Kirkpatrick J, Ball NJ, Hilditch L, Yap MW, Rosenthal PB, Stoye JP, Taylor IA, (2014). Structural studies of postentry restriction factors reveal antiparallel dimers that enable avid binding to the HIV-1 capsid lattice. Proc. Natl. Acad. Sci. U.S.A 111, 9609–9614. [PubMed: 24979782]

32. Liu C, Perilla JR, Ning J, Lu M, Hou G, Ramalho R, Himes BA, Zhao G, Bedwell GJ, Byeon IJ, Ahn J, Gronenborn AM, Prevelige PE, Rousso I, Aiken C, Polenova T, Schulten K, Zhang P, (2016). Cyclophilin A stabilizes the HIV-1 capsid through a novel non-canonical binding site. Nature Commun 7, 10714. [PubMed: 26940118]

33. Wagner JM, Roganowicz MD, Skorupka K, Alam SL, Christensen D, Doss G, Wan Y, Frank GA, Ganser-Pornillos BK, Sundquist WI, Pornillos O, (2016). Mechanism of B-box 2 domain-mediated higher-order assembly of the retroviral restriction factor TRIM5α. eLife 5, e16309. [PubMed: 27253059]

34. Wagner JM, Christensen DE, Bhattacharya A, Dawidziak DM, Roganowicz MD, Wan Y, Pumroy RA, Demeler B, Ivanov DN, Ganser-Pornillos BK, Sundquist WI, Pornillos O, (2018). General model for retroviral capsid pattern recognition by TRIM5 proteins. J. Virol 92 e01563–17. [PubMed: 29187540]

35. Ning J, Zhong Z, Fischer DK, Harris G, Watkins SC, Ambrose Z, Zhang P, (2018). Truncated CPSF6 forms higher-order complexes that bind and disrupt HIV-1 capsid. J. Virol 92, e00368–e00418. [PubMed: 29643241]

36. Wei G, Iqbal N, Courouble VV, Francis AC, Singh PK, Hudait A, Annamalai AS, Bester S, Huang SW, Shkriabai N, Briganti L, Haney R, KewalRamani VN, Voth GA, Engelman AN, Melikyan GB, Griffin PR, Asturias F, Kvaratskhelia M, (2022). Prion-like low complexity regions enable avid virus-host interactions during HIV-1 infection. Nature Commun 13, 5879. [PubMed: 36202818]

37. Eschbach JE, Ellliott JL, Li W, Zadrozny KK, Davis K, Mohammed SJ, Lawson DQ, Pornillos O, Engelman AN, Kutluay SB, (2020). Capsid lattice destabilization leads to premature loss of the viral genome and integrase enzyme during HIV-1 infection. J. Virol 95, e00984–e01020. [PubMed: 33115869]

38. Schindelin J, Arganda-Carreras I, Frise E, Kaynig V, Longair M, Pietzsch T, Preibisch S, Rueden C, Saalfeld S, Schmid B, Tinevez J, White DJ, Hartenstein V, Eliceiri K, Tomancak P, Cardona A, (2012). Fiji: an open-source platform for biological-image analysis. Nature Methods 9, 676–682. [PubMed: 22743772]

39. Punjani A, Rubinstein JL, Fleet DJ, Brubaker MA, (2017). cryoSPARC: algorithms for rapid unsupervised cryo-EM structure determination. Nature Methods 14, 290–296. [PubMed: 28165473]

40. Zheng SQ, Palovcak E, Armache J-P, Verba KA, Cheng Y, Agard DA, (2017). MotionCor2: anisotropic correction of beam-induced motion for improved cryo-electron microscopy. Nature Methods 14, 331–332. [PubMed: 28250466]

41. Rohou A, Grigorieff N, (2015). CTFFIND4: Fast and accurate defocus estimation from electron micrographs. J. Struct. Biol 192, 216–221. [PubMed: 26278980]

42. Emsley P, Lohkamp B, Scott WG, Cowtan K, (2010). Features and development of Coot. Acta Crystallogr. D Biol. Crystallogr 66, 486–501. [PubMed: 20383002]

43. Liebschner D, Afonine PV, Baker ML, Bunkóczi G, Chen VB, Croll TI, Hintze B, Hung LW, Jain S, McCoy AJ, Moriarty NW, Oeffner RD, Poon BK, Prisant MG, Read RJ, Richardson JS, Richardson DC, Sammito MD, Sobolev OV, Stockwell DH, Terwilliger TC, Urzhumtsev AG, Videau LL, Williams CJ, Adams PD, (2019). Macromolecular structure determination using X-

rays, neutrons and electrons: recent developments in Phenix. Acta Crystallogr. D Biol. Crystallogr 75, 861–877.

44. Jumper J, Evans R, Pritzel A, Green T, Figurnov M, Ronneberger O, Tunyasuvunakool K, Bates R, Žídek A, Potapenko A, Bridgland A, Meyer C, Kohl SAA, Ballard AJ, Cowie A, Romera-Paredes B, Nikolov S, Jain R, Adler J, Back T, Petersen S, Reiman D, Clancy E, Zielinksi M, Steinegger M, Pacholska M, Berghammer T, Bodenstein S, Silver D, Vinyals O, Senior AW, Kavukcuoglu K, Kohli P, Hassabis D, (2021). Highly accurate protein structure prediction with AlphaFold. Nature 596, 583–589. [PubMed: 34265844]

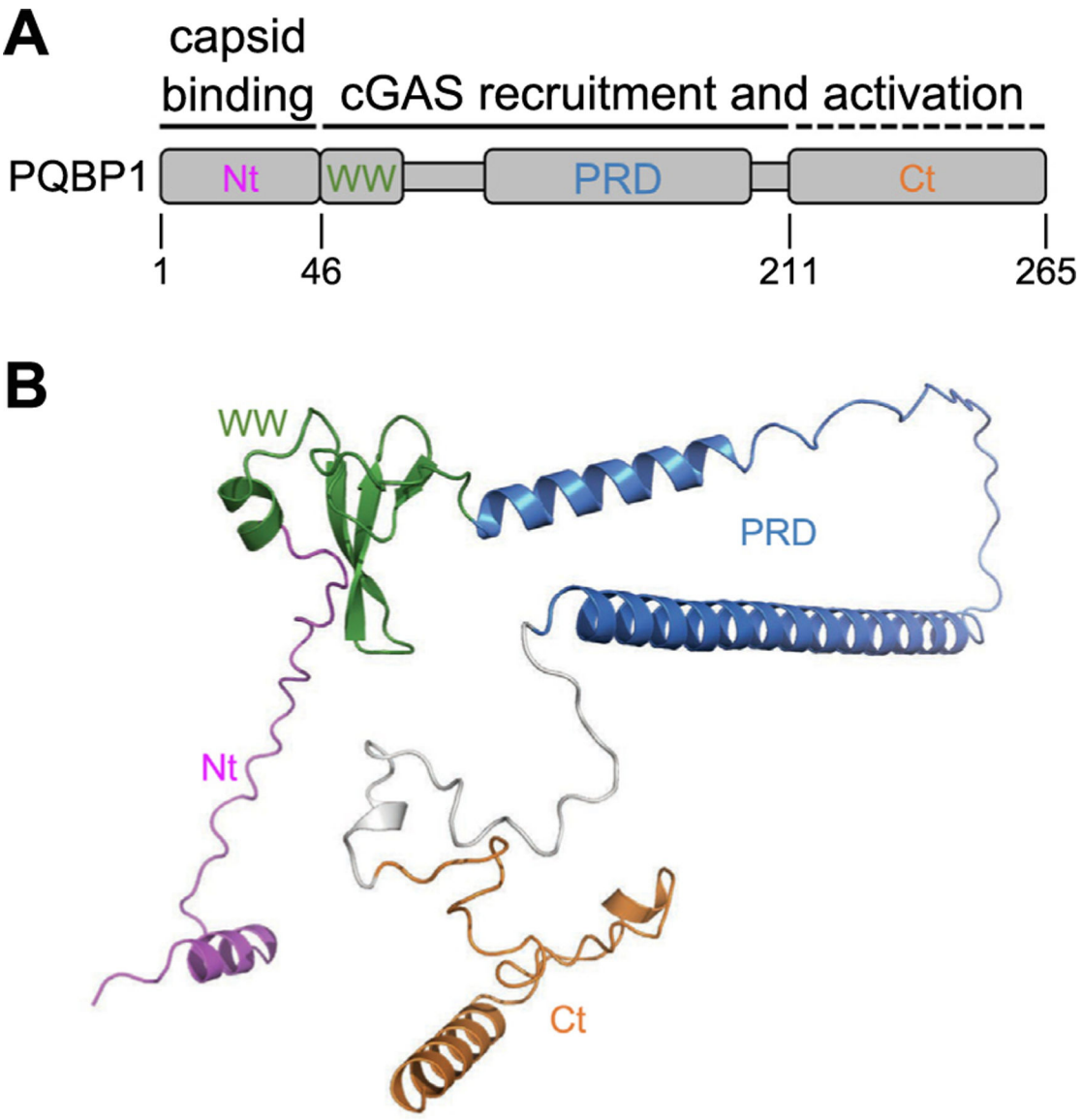

Figure 1.

PQBP1 is an intrinsically disordered protein (IDP). **(A)** Schematic of the protein primary sequence. Functionally-defined regions for capsid binding and cGAS recruitment and activation are indicated. **(B)** Ribbons representation of predicted PQBP1 structure by AlphaFold.[44] Functional domains are shown in different colors and labeled.

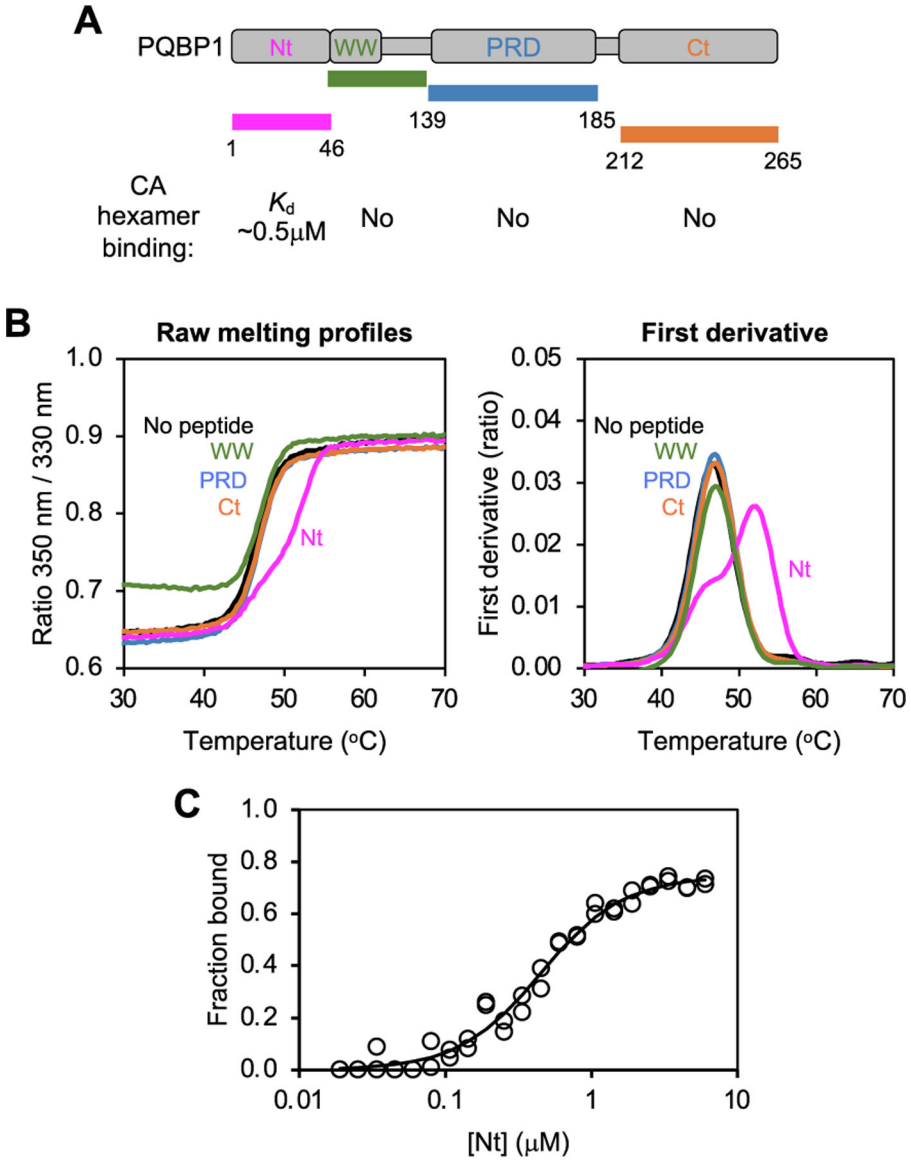

Figure 2.

The N-terminal (Nt) region of PQBP1 directly binds soluble disulfide-stabilized HIV-1 CA hexamer. **(A)** Schematic of synthetic PQBP1 peptides spanning Nt, WW, PRD (polar-rich domain), and Ct (C-terminal region). **(B)** NanoDSF raw melting profiles (left panel) and first derivative curves (right panel) of HIV-1 CA hexamer in the presence of the indicated PQBP1 constructs. Results are representative of at least two experiments. **(C)** Nt binding data were fit to a simple binding model. Results are representative of 4 independent experiments, each with 2–3 replicates.

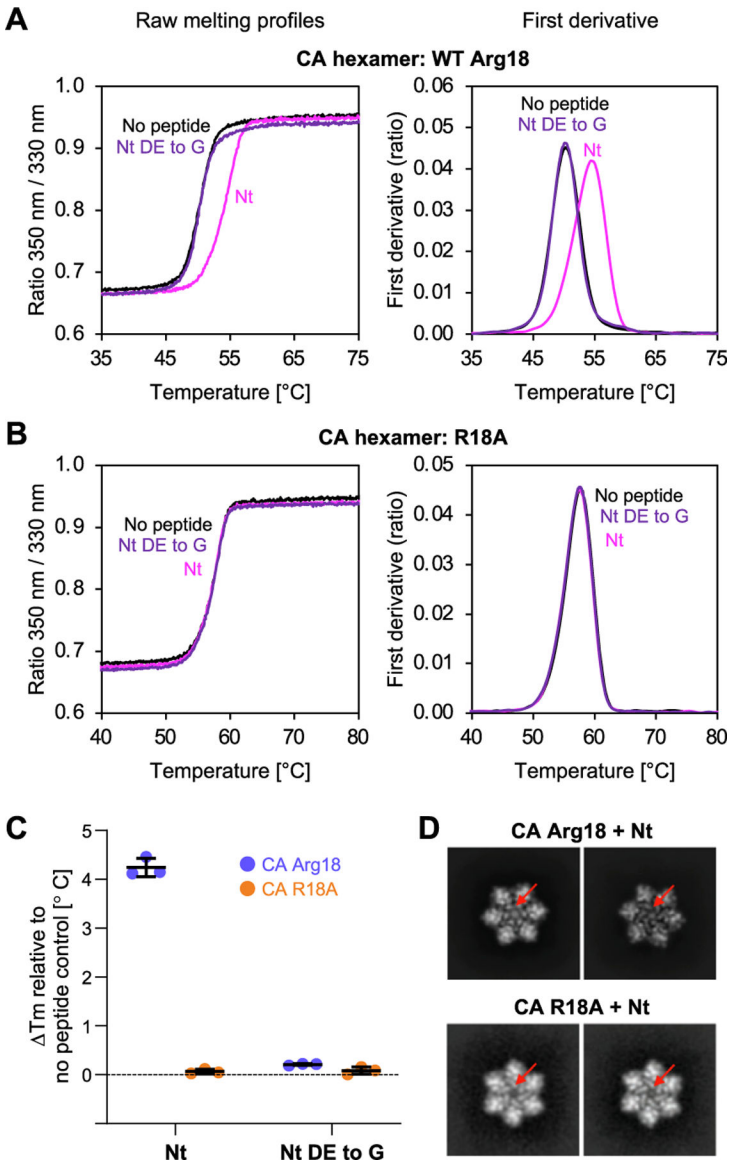

Figure 3.

PQBP1 Nt binding to the hexamer is mediated by charge interactions. **(A)** and **(B)** NanoDSF raw melting profiles (left panels) and first derivative curves (right panels) of HIV-1 CA hexamer (0.83 μM) containing non-mutated Arg18 (A) or R18A mutation (B), after incubation with 5 μM Nt peptide (magenta), or Nt DE-to-G mutant (purple), or without peptide (black). Data are representative of at least 3 technical replicates. **(C)** Summary of thermostabilization data, presented as mean ± S.D. of three independent experiments. **(D)** Representative 2D class averages of the indicated CA hexamers after incubation with 3-fold excess Nt peptide. Red arrows indicate the central channel.

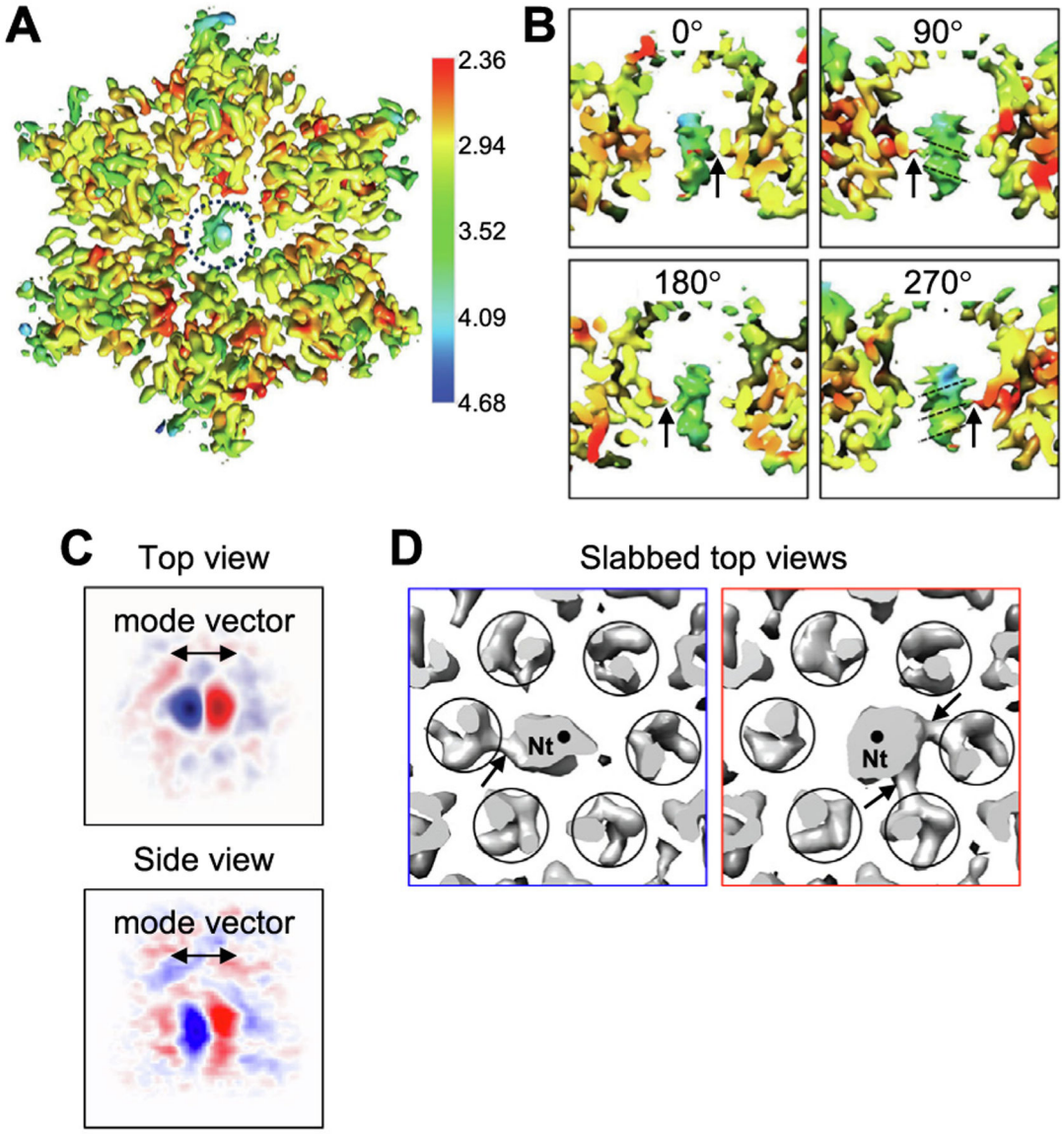

Figure 4.

CryoEM structure of the CA hexamer bound to Nt. **(A)** Top view of the consensus map refined with C1 symmetry, colored according to local resolution. The peptide in the central channel is encircled. **(B)** Orthogonal side views of the peptide density. Arrows indicate apparent contacts between the peptide and Arg18. Dashed lines indicate evenly spaced ridges that we interpret to be consistent with a predominant helical configuration. **(C)** Orthogonal views of central slices through the major 3D variability component for the consensus map, as determined by 3DVA analysis. Positive (red) and negative (blue) values indicate different positions of the peptide relative to the central hexamer channel. **(D)** Reconstructions of particle subsets, without further alignment, revealing two peptide orientations determined by 3DVA. Circles indicate densities for CA helix 1 surrounding the central channel. Black dots indicate the central axis of the hexamer channel. Arrows indicate clearly defined contacts between the peptide and Arg18.

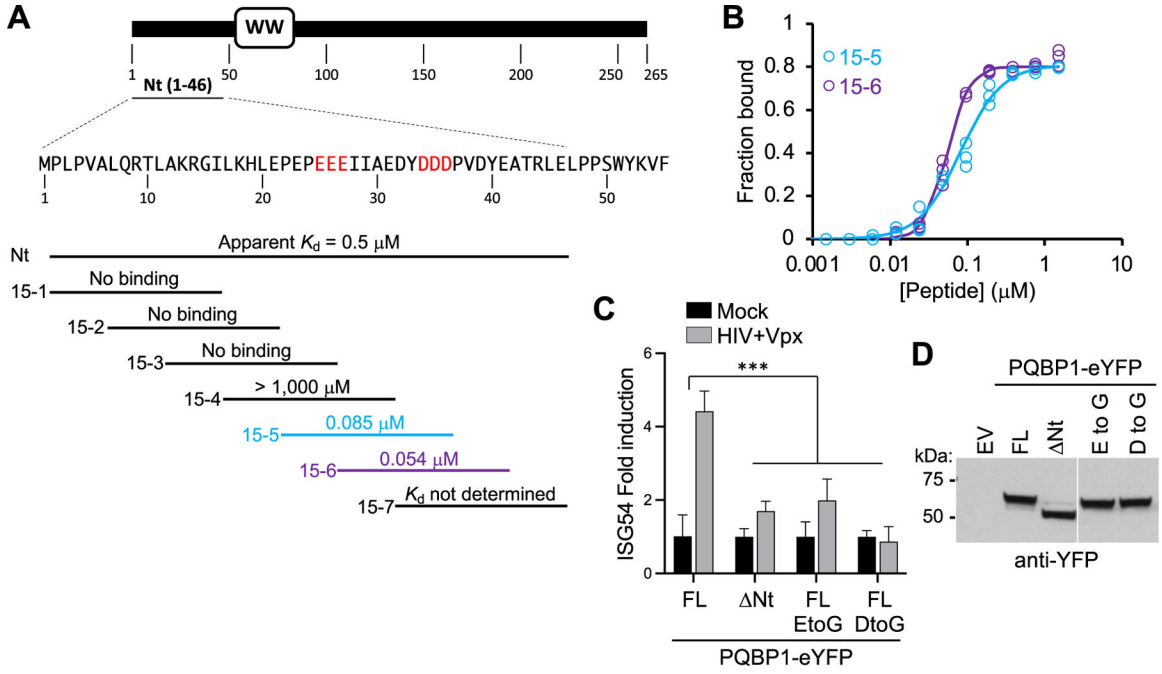

Figure 5.

High-affinity hexamer binding requires a tri-aspartate motif in Nt. **(A)** Sequence of Nt and positions of 15-mer peptides. **(B)** Binding data for peptides 15–5 and 15–6. Data are representative of three independent experiments, each in three replicates. **(C)** HIV-dependent ISG54 induction by the indicated PQBP1-eYFP constructs in differentiated THP-1 cells, shown as mean ± S.D. Experiments were done in biological triplicate; shown is representative of two independent experiments. ***, $p < 0.001$ (two-way ANOVA). **(D)** Anti-YFP immunoblot of THP-1 whole cell lysates to detect expression levels of indicated PQBP1-eYFP constructs. EV, empty vector.

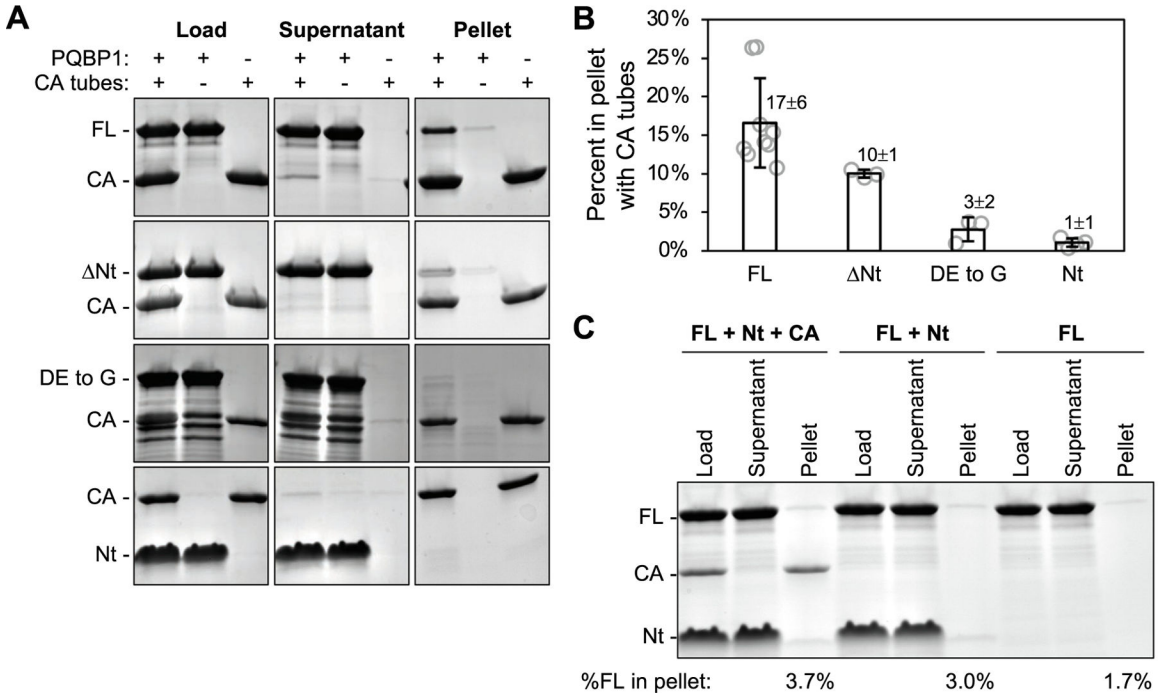

Figure 6.

PQBP1 binding to the HIV-1 capsid lattice in vitro. **(A)** Indicated combinations of PQBP1 constructs (50 μM) and disulfide-stabilized CA tubes (50 μM in terms of CA subunits, which is equivalent to 8.3 μM of hexamer) were incubated for 1 h at room temperature, then centrifuged. Load, Supernatant, and Pellet fractions were analyzed using SDS-PAGE and Coomassie staining. Representative of 9 (FL, full-length PQBP1), 3 (ΔNt mutant), 3 (DE-to-G mutant), or 4 (Nt peptide) experiments. **(B)** Band intensities for pelleted PQBP1 in the presence of CA tubes after subtraction of matching negative controls in the absence of CA tubes, reported as mean ± S.D. **(C)** FL PQBP1 was incubated with Nt peptide and/or CA tubes as indicated, for 1 h at room temperature prior to centrifugation. Numbers indicate percentage of input FL PQBP1 in the pellet fraction. Representative of 2 independent experiments.

Table 1

Binding parameters for PQBP1 peptides and disulfide-stabilized HIV-1 CA hexamer

PQBP1 peptide	Apparent K_d (nM)	Hill coefficient	CA sp. activity
Nt	503 ± 66	1.6 ± 0.1	0.8
15–5	85.0 ± 1.0	1.8 ± 0.4	0.8
15–6	54.0 ± 0.4	3.0 ± 0.2	0.8

Note: K_d and Hill coefficient were treated as floating parameters during fitting, but not CA specific activity. Values are presented as mean ± S.D. of four (Nt) or three (15–5 and 15–6) independent determinations.

Table 2

CryoEM data collection, structure refinement, and coordinate modeling statistics.

Data collection			
Magnification	81,000×		
Voltage	300 kV		
Electron dose	50 e/Å^2		
Defocus range	0.5 to 2.5 μm		
Pixel size	1.08 Å		
Image processing and map calculation			
	Consensus	**3DVA Frame 0**	**3DVA Frame 1**
Symmetry imposed	C1	C1	C1
No. of particles	312,788	154,820	157,280
Map resolution / FSC threshold	3.3 Å / 0.143	3.5 Å / 0.143	3.5 Å / 0.143
Map resolution range* (Å)	2.4–31.4 Å	2.3–9.7 Å	2.3–10.0 Å
Coordinate modeling and refinement			
Initial model	PDB 3H47		
Model resolution / threshold	3.2 Å / 0.143		
Map sharpening B-factor	109 Å^2		
Mean real-space cross-correlation (CC)	0.81		
No. of non-hydrogen atoms	9,678		
Protein residues	1,260		
Mean B-factor	74.26 Å^2		
RMSD bond lengths	0.002 Å		
RMSD bond angles	0.443°		
MolProbity score / clash score	1.61 / 4.89		
Poor rotamers	2.71%		
Ramachandran favored / outliers / z-score	98.9% / 0% / 2.36		

*Determined using the Local Resolution job in cryoSPARC, with FSC cut-off set a 0.143.